

# Physics Informed Neural Network for Health Monitoring of an Air Preheater

Vishal Jadhav<sup>1</sup>, Anirudh Deodhar<sup>2</sup>, Ashit Gupta<sup>3</sup>, and Venkataramana Runkana<sup>4</sup>

<sup>1,2,3,4</sup>*TCS Research, Tata Consultancy Services Limited, Pune, India*

*vi.suja@tcs.com*  
*anirudh.deodhar@tcs.com*  
*ashit.gupta@tcs.com*  
*venkat.runkana@tcs.com*

## ABSTRACT

Air Preheater (APH) is a regenerative heat exchanger employed in thermal power plants to save fuel by improving their thermal efficiency. Monitoring the health of APH vis-a-vis its fouling is critical because fouling often results in forced outages of the power plant, incurring huge revenue losses. APH fouling is a complex thermo-chemical phenomenon governed by flue gas composition, operating temperatures, fuel type and ambient conditions. Absence of sensors within the APH make it difficult to estimate the level of fouling and its progression even for an experienced operator. Attempts to estimate APH fouling in real-time via modeling are scarce. Here we present a physics-informed neural network (PINN) that tracks the health of an APH by real-time estimation of fouling conditions within the APH as a function of real-time sensor measurements. To account for multi-fluid operation in a multi-sector design of APH, the domain is decomposed into several sub-domains. PINN is applied to each sub-domain and the overall solution is ensured by applying continuity conditions at the sub-domain interfaces. The model predicts the interior temperatures and fouling zones within the APH using external sensor measurements such as air temperature and gas composition. The model predictions are consistent with physics and yet computationally efficient in run-time. The model does not need sensor data but can be improved further by accommodating available sensor data. The real-time predictions by the model improve operator's visibility in fouling. The predictions can be used further for estimating the remaining useful cycle life of the APH, thereby avoiding forced outages. The model can easily be integrated with the digital twin of an APH for its predictive maintenance.

## 1. INTRODUCTION

Air preheaters (APH) are used in thermal power plants for improving thermal efficiency by recovering the excess heat from boiler exhaust gases. APH fouling is a serious and recurring problem that often causes unplanned outages of the plant incurring huge revenue losses. Complex thermo-chemical phenomena in fouling and lack of sensors within APH, make it difficult to monitor the fouling in real-time requiring predictive models.

APH typically comprises two or three successive layers of matrix that enable effective heat transfer by increasing the surface area per unit volume. This rotating metallic matrix extracts heat from the hot flue gas and passes it on to the ambient air flowing in a countercurrent manner with respect to the gas. Depending upon the number of air streams, APH can have a 2-sector or a 3-sector arrangement. Fouling is caused by gradual deposition of a chemical compound called ammonium bisulfate (ABS), formation of which is predominantly influenced by the internal temperature profile within APH and the gas composition (ammonia  $\text{NH}_3$ , sulfur trioxide  $\text{SO}_3$  and ash). Several ABS formation and deposition studies (Muzio, Bogseth, Himes, Chien, & Dunn-Rankin, 2017; Menasha, Dunn-Rankin, Muzio, & Stallings, 2011; Zhou, Zhang, Deng, & Ma, 2016) have revealed that the gas temperature profile within APH influences not only the magnitude of fouling but also the location of fouling and in turn governs its overall progression. Although no models have been developed for estimating chemical formation and deposition directly, several models capturing thermal phenomena have been developed based on first principles including Computational Fluid Dynamics (CFD) (Li, 1983; Skiepko, 1988; Drobnic, Oman & Tuma 2006, Wang, Bu, Li, Tang, & Che, 2019; Heidari-Kaydan, Hajidavalloo, & Mehrzad, 2021). However, most of the models are computationally expensive with significantly high inference time and hence not amenable for real-time applications.

Vishal Jadhav et al. This is an open-access article distributed under the terms of the Creative Commons Attribution 3.0 United States License, which permits unrestricted use, distribution, and reproduction in any medium, provided the original author and source are credited.

Empirical models proposed for estimating propensity of fouling (Burke & Johnson 1982; Wang et al. 2019; Chen, Xu, Yang, Wang, & Wang 2020) also require the internal temperature profile of APH for accurate estimations. Data-driven models based on machine or deep learning have been explored for fouling estimation (Sundar, Rajagopal, Zhao, Kuntumalla, Meng, Chang, Shao, Ferreira, Miljkovic, Sinha, & Salapaka, 2020; and Gupta, Jadhav, Patil, Deodhar, & Runkana, 2021). However, these models are heavily dependent on the quality and availability of data. In absence of sensor measurements inside the APH and overall difficulty in obtaining sufficient industrial data, purely data-driven models are not effective. In addition, often the inferences from purely data-driven models may defy physical principles.

Physics informed neural networks (PINNs) (Raissi, Perdikaris, & Karniadakis 2019) are gaining popularity as a viable alternative to address limitations and harness the power of both physics-based and data-driven models. PINNs are a type of universal function approximators that are trained by imposing governing partial differential equations as constraints. These constraints are applied by introducing governing equation residuals and boundary or initial conditions in the loss function. This approach enables the neural network to incorporate domain knowledge in the learning process and learns virtually without any data in a semi-supervised manner. PINNs make the model more flexible by eliminating a fixed mesh typically required in a physics-based numerical solver, while remaining physically consistent.

Lagaris, Likas and Fotiadis (1998) were the first to introduce neural networks to solve boundary value problems for partial differential equations (PDEs). Raissi, et al. (2019) introduced the concept of incorporating governing PDEs in the loss function of a deep neural network to solve both forward and inverse problems. Since then, PINN has been used for solving various scientific problems in several domains (Cuomo, Di Cola, Giampaolo, Rozza, Raissi, & Piccialli, 2022) including fluid flow (Cai, Mao, Wang, Yin & Karniadakis, 2022) and heat transfer (Cai, Wang, Wang, Perdikaris & Karniadakis, 2021).

A few limitations of the PINNs have been recently highlighted by Cuomo et al. (2022) in their review. Even though the inference time for PINN models is considerably low, high training time and significant convergence difficulties in complex scenarios limit their implementation in real life applications (Jagtap & Karniadakis, 2020). Shukla, Jagtap and Karniadakis (2021) suggested the distributed framework for training PINN models to reduce the training time. Domain decomposition is one such strategy of distributed framework usually adapted to reduce the complexity of training PINNs (Heinlein, Klawonn, Lanser, & Weber, 2021). cPINN (Jagtap, Kharazmi, & Karniadakis, 2020) and xPINN (Jagtap & Karniadakis, 2020) networks employ the domain decomposition strategy to get accurate solutions of complex nonlinear conservation laws. Recently,

Moseley, Markham, and Nissen-Meyer (2021) proposed the domain decomposition approach to solve large multiscale problems. Another limitation of current PINN techniques is that they fail to generalize over dynamically changing boundary conditions (Cuomo et al. 2022) for governing differential equations, a scenario often found in industrial applications.

PINNs trained over single set of boundary conditions cannot be used in application where parameter values change dynamically (Wang, Planas, Chandramowlishwaran and Bostanabad, 2021). Wang et al. (2021) proposed a ‘train once use forever’ algorithm comprising of a combination of GFNet and Mosaic Flow Predictor that enables one time training of a neural network that can generalize over arbitrary boundary conditions as well as arbitrary domain shapes. Meta learning (Penwarden, Zhe, Narayan, & Kirby, 2021) and hypernetwork (Belbute-Peres, Yi-fan, & Fei, 2021) approaches have also been suggested for adapting PINNs to dynamic boundary conditions. Chakraborty (2021) suggested the use of transfer learning for training of multi fidelity PINNs. Desai, Mattheakis, Joy, Protopapas, and Roberts, (2021) has presented use of transfer learning with pre-trained neural network for one-shot inference for linear system of both ordinary and partial differential equations.

In the present work, we apply some of these concepts to develop a PINN model for real-time health monitoring of an industrial APH. The base PINN model is developed by decomposing the APH into three sub-domains and stitching the individual sub-domain PINNs by applying continuity conditions at the respective interfaces. The model solves a set of two-dimensional governing equations for capturing the heat transfer phenomenon and predicts the internal temperature profile of APH for air, gas and metal based on the external boundary conditions such as inlet air and gas temperatures. Boundary conditions used to solve governing equations herein refers to inlet gas and air temperatures, which are typically known through sensor measurements. Fouling propensity is a function of temperatures and chemical concentrations in APH. Online monitoring of fouling propensity can be enabled through PINN models trained for different boundary conditions. However, in online applications temperatures of gas and air, flow rates and composition of flue gas vary significantly. This results in numerous combinations of conditions and for each such condition offline simulation or training of PINN is not practical. To address this challenge, a transfer learning framework is used which enables computationally inexpensive and near real-time re-training and inference from the network for a change in boundary conditions, making the model suitable for real-time industrial application. The model inference is shown to be as accurate as and significantly faster than corresponding physics-based numerical solution. In current study finite combination of temperatures (9 cases) are considered to demonstrate the use of transfer learning to speed up the training time. However, in practice numerous

combinations of temperatures or other parameters are possible. Transfer learning framework proposed will be useful for online estimation of temperature profile and fouling propensity monitoring in industrial application. Online estimation of temperature profile further can also be used for digital twin applications wherein real time predictions are used for process optimization, maintenance decisions, safety related decisions along with monitoring.

## 2. METHODOLOGY

### 2.1. Governing Equations for APH heat transfer

Figure 1 shows the schematic of APH of height  $H$ , outer diameter  $d_o$ , inner diameter  $d_i$  and sector angles of  $\beta_g, \beta_{a1}, \beta_{a2}$  for flue gas, primary air, and secondary air flow. Flue gas enters APH from the top whereas primary air and secondary air enter from bottom. The metallic matrix rotates at  $\omega$  revolutions per minute (rpm).

High temperature flue gas enters from top and heats the matrix, which in turn rotates and transfers this heat to the cold ambient air entering from bottom. While convection dominates the heat transfer between fluids and metal, conduction contributes significantly to the heat transfer within metal. In the current work, we consider a two-dimensional formulation (tangential and axial direction) for solving thermal governing equations inside the APH. Heat transfer in the radial direction is assumed to be constant and hence not accounted for in the governing equations (Skiępko 1988).

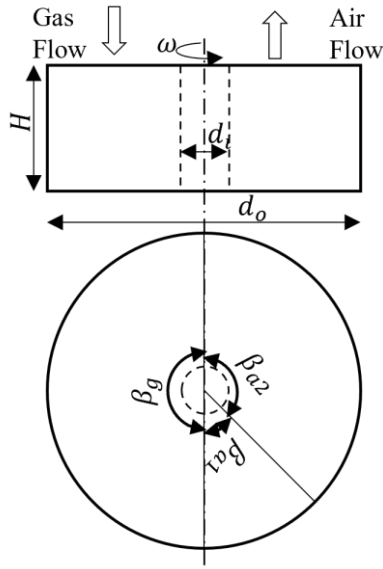


Figure 1 APH Schematic

The computational domain considered is shown in Figure 2. Due to the presence of different fluid (gas & air) channels in

the tangential direction, fluid temperature profile would be discontinuous. PINN models are known to encounter difficulties in generalizing for such solution discontinuities (Jagtap et al. 2020). Therefore, entire domain ( $\Omega$ ) is divided into three subdomains presented as gas side subdomain ( $\Omega_g$ ), primary air side sub domain ( $\Omega_{a1}$ ), and secondary air side sub domain ( $\Omega_{a2}$ ), as shown in Figure 2. Each sub domain coordinates are normalized from 0 to 1 for both axial and tangential directions. It can be noted that, for gas side subdomain positive axial direction is from top to bottom which is same as gas flow direction. Similarly, for primary air side and secondary air side subdomain, positive axial direction is from bottom to top which is same as flow direction for primary and secondary air. Positive tangential direction is considered from left to right for all subdomains, which is same as rotational direction of matrix. For simplicity, all metal matrix layers are assumed to be made of a single homogeneous material, however the approach mentioned can be extended to a multi material matrix APH as well.

Eqs. (1-6) represent the non-dimensionalised governing equations for heat transfer between the fluids and the metal (Skiępko 1988). Here, subscript  $m, g, a1, a2$  are used to represent matrix, gas, primary air and secondary air respectively. Subscript  $m_g, m_{a1}, m_{a2}$  are used to represent matrix in gas, primary air and secondary air domain respectively. Number of transfer units ( $NTU$ ) and Peclet number ( $Pe$ ), are used to non dimensionalize the governing equations (Skiępko 1988).

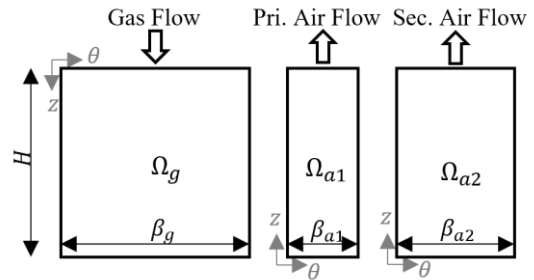


Figure 2 Computational domain for Air Preheater

$$\frac{\partial T_{m_g}}{\partial \theta} = NTU_{m_g} (T_g - T_{m_g}) + Pe_{m_g}^{-1} \frac{\partial^2 T_{m_g}}{\partial z^2} \quad (1)$$

$$\frac{\partial T_g}{\partial z} = NTU_g (T_{m_g} - T_g) \quad (2)$$

$$\frac{\partial T_{m_{a1}}}{\partial \theta} = NTU_{m_{a1}} (T_{a1} - T_{m_{a1}}) + Pe_{m_{a1}}^{-1} \frac{\partial^2 T_{m_{a1}}}{\partial z^2} \quad (3)$$

$$\frac{\partial T_{a1}}{\partial z} = NTU_{a1}(T_{m_{a1}} - T_{a1}) \quad (4)$$

$$\frac{\partial T_{m_{a2}}}{\partial \theta} = NTU_{m_{a2}}(T_{a2} - T_{m_{a2}}) + Pe_{m_{a2}}^{-1} \frac{\partial^2 T_{m_{a2}}}{\partial z^2} \quad (5)$$

$$\frac{\partial T_{a2}}{\partial z} = NTU_{a2}(T_{m_{a2}} - T_{a2}) \quad (6)$$

Temperature measurements of gas and air at the respective inlets are used as boundary conditions to solve the governing equations. Eqs. (7-9) represent the boundary conditions.

$$T_g(\theta, z = 0) = T_{gin} \quad (7)$$

$$T_{a1}(\theta, z = 0) = T_{a1in} \quad (8)$$

$$T_{a2}(\theta, z = 0) = T_{a2in} \quad (9)$$

Along with boundary conditions, continuity constraints due to rotation of matrix from gas side to primary air side, primary air side to secondary air side and secondary air side to gas side again are applied as shown in eqs. (10-12)

$$T_{m_g}(\theta = 0, z) = T_{m_{a2}}(\theta = 1, 1 - z) \quad (10)$$

$$T_{m_g}(\theta = 1, z) = T_{m_{a1}}(\theta = 0, 1 - z) \quad (11)$$

$$T_{m_{a1}}(\theta = 1, z) = T_{m_{a2}}(\theta = 0, z) \quad (12)$$

As axial heat conduction in metal is zero at the end of metallic layer additional matrix temperature gradient constraints are imposed as shown eqs. (13-15)

$$\frac{\partial T_{m_g}[\theta, (z = 0 \text{ and } 1)]}{\partial z} = 0 \quad (13)$$

$$\frac{\partial T_{m_{a1}}[\theta, (z = 0 \text{ and } 1)]}{\partial z} = 0 \quad (14)$$

$$\frac{\partial T_{m_{a2}}[\theta, (z = 0 \text{ and } 1)]}{\partial z} = 0 \quad (15)$$

## 2.2. Physics Informed Neural Network

### 2.2.1. Neural Network Architecture

Base PINN model for APH consists of a deep neural network (DNN) for each of the subdomains  $p$  in APH (i.e.,  $\Omega_g, \Omega_{a1}, \Omega_{a2}$ ). The spatial co-ordinates  $(\theta, z)$  are the inputs to each network and the outputs are fluid temperature ( $T_f$ ) (air or gas) and matrix temperature ( $T_m$ ) for each sub-domain respectively. Let  $\mathcal{N}^L: \mathbb{R}^{D_i} \rightarrow \mathbb{R}^{D_o}$  be a deep neural network of  $L$  layers and  $N_k$  neurons in  $k^{th}$  layer ( $N_0 = D_i$  and  $N_L = D_o$ ). The weight matrix and bias vector in the  $k^{th}$  layer ( $1 \leq k \leq L$ ) are denoted by  $\mathbf{W}^k \in \mathbb{R}^{N_k \times N_{k-1}}$  and  $\mathbf{b}^k \in \mathbb{R}^{N_k}$  respectively. Input vector is denoted as  $\mathbf{x} \in \mathbb{R}^{D_i}$ , output vector at  $k^{th}$  layer is denoted as  $\mathcal{N}^k(\mathbf{x})$  and  $\mathcal{N}^0(\mathbf{x}) = \mathbf{x}$ . Activation function is denoted as  $\Phi$ . DNN is defined by eq. (16):

$$\mathcal{N}^k(\mathbf{x}) = \Phi(\mathbf{W}^k \mathcal{N}^{k-1}(\mathbf{x}) + \mathbf{b}^k), \quad 1 \leq k \leq L \quad (16)$$

Let,  $\Theta = \{\mathbf{W}^k, \mathbf{b}^k\}$  be a collection of all weights and biases. Then output of neural network is given by eq. (17).

$$u_{\Theta}(\mathbf{x}) = \mathcal{N}^L(\mathbf{x}; \Theta) \quad (17)$$

Figure 3 shows the schematic of PINN architecture, wherein three deep neural networks are used for each sub-domain respectively. For each sub domain, the output of individual deep neural network is given as

$$u_{i_{\Theta}}(\mathbf{x}) = \mathcal{N}_i^L(\mathbf{x}; \Theta), \forall i = 1, 2, 3 \quad (18)$$

The final solution will be given as

$$u_{\Theta}(\mathbf{x}) = \bigcup_{i=1}^3 u_{i_{\Theta}}(\mathbf{x}) \quad (19)$$

### 2.2.2. Sub domain Loss Function

Total loss for PINN comprises of mean squared error ( $MSE$ ) due to residuals of governing equations calculated using collocation points ( $MSE_{\mathcal{F}_p}$ ), loss due to boundary condition calculated using boundary points ( $MSE_{bc_p}$ ), MSE loss due to interface condition calculated at interface points ( $MSE_{ic_p}$ ) and MSE loss due to matrix temperature gradient calculated at top and bottom points of each sub domain ( $MSE_{grad_p}$ ). Mean squared error for different components of sub domain  $p$  is calculated using eqs. (20-23):

$$MSE_{\mathcal{F}_p} = \frac{1}{N_{\mathcal{F}_p}} \sum_{i=1}^{N_{\mathcal{F}_p}} \left| \mathcal{F}(\theta_{\mathcal{F}_p}^i, z_{\mathcal{F}_p}^i) \right|^2 \quad (20)$$

$$MSE_{ic_p} = \frac{1}{N_{ic_p}} \sum_{i=1}^{N_{ic_p}} \left| T_{m_p}(\theta_{ic_p}^i, z_{ic_p}^i) - T_{m_{p^+}}(\theta_{ic_p}^i, z_{ic_p}^i) \right|^2 \quad (21)$$

$$MSE_{bc_p} = \frac{1}{N_{bc_p}} \sum_{i=1}^{N_{bc_p}} \left| T_{f_p}^i - T_{f_p}(\theta_{bc_p}^i, z_{bc_p}^i) \right|^2 \quad (22)$$

$$MSE_{grad_p} = \frac{1}{N_{grad_p}} \sum_{i=1}^{N_{grad_p}} \left| \frac{\partial T_{m_p}(\theta_{grad_p}^i, z_{grad_p}^i)}{\partial z} \right|^2 \quad (23)$$

Where,  $\mathcal{F}$  is the residual of governing PDEs, subscript  $p^+$  indicates the neighboring subdomain to subdomain  $p$ ,  $N_{\mathcal{F}_p}, N_{ic_p}, N_{bc_p}, N_{grad_p}$  represents number of collocation points, number of interface condition points, number of boundary condition points and number of matrix temperature gradient condition points in  $p^{th}$  subdomain respectively.  $(\theta_{\mathcal{F}_p}^i, z_{\mathcal{F}_p}^i)$ ,  $(\theta_{bc_p}^i, z_{bc_p}^i)$  and  $(\theta_{grad_p}^i, z_{grad_p}^i)$  represents the co-ordinates of the residual points, boundary condition points and gradient condition points for  $p^{th}$  sub domain.  $(\theta_{ic_p}^i, z_{ic_p}^i)$  represents the common interface points of two neighboring subdomains  $p$  and  $p^+$ . Loss for  $p^{th}$  subdomain is given in eq. (24).

$$\mathcal{L}(\Theta)_p = MSE_{\mathcal{F}_p} + MSE_{ic_p} + MSE_{bc_p} + MSE_{grad_p} \quad (24)$$

Total loss for PINN is given by eq. (25), where subscript  $g, a1, a2$  represents subdomain for gas, primary air, and secondary air.

$$\mathcal{L}(\Theta) = \mathcal{L}(\Theta)_g + \mathcal{L}(\Theta)_{a1} + \mathcal{L}(\Theta)_{a2} \quad (25)$$

DNN for each subdomain consist of one input layer (two neurons), two hidden layers (with 16 neurons in each layer) and one output layer (two neurons). Activation function used for hidden layers and output layer is tanh. Gradients for evaluating the residual equation are calculated using auto differentiation feature (Baydin, Pearlmutter, Radul, & Siskind, 2018). Adam optimizer is used to train PINN model mean squared error is used as loss metric. Additionally, reducing learning rate callback and early stopping callback features from tensorflow were used for better control while training. If the loss does not reduce compared to the best loss value for 50 epochs, learning rate is reduced by factor of 0.1 with reducing learning rate callback. Also, early stopping callback was used to stop the training if the training loss does not improve for 100 epochs. Machine used for numerical simulation and PINN model training has specifications as follows: AMD Ryzen 5 2500U processor with Radeon Vega Mobile Gfx 2.00 GHz, RAM of 24 GB and 64-bit operating system.

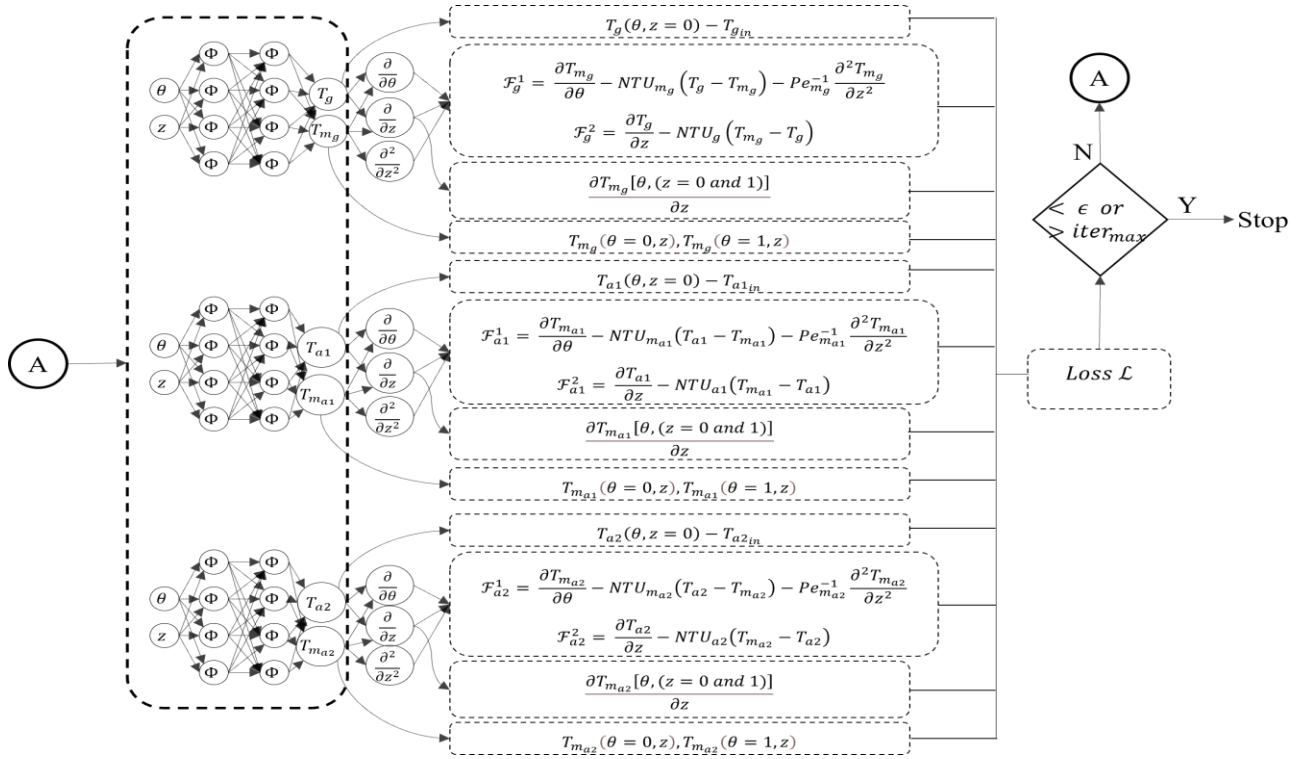


Figure 3 PINN Architecture

### 2.3. Transfer Learning Based Dynamic Prediction using PINN

The base PINN described above can predict the internal temperatures accurately only for the set of boundary conditions it is trained with. However, industrial scenario requires a model that can predict the temperatures dynamically for varying boundary conditions in near real-time. To enable quick re-training and inference for a different boundary condition, a transfer learning inspired approach is utilized. The weights of the base PINN model trained for benchmark boundary condition are used for initialization and instead of training all those weights, weights and bias for the input layer and first hidden layer are frozen for each DNN of each subdomain. This follows from the assumption that layer 1 of each DNN captures the benchmark physical phenomena sufficiently and the second layer manipulates the inference for the altered boundary condition. The accuracy and computational time based on this method is later compared with the traditional physics-based numerical solver and the PINN model with all layers trainable.

### 2.4. Health Monitoring using inference from PINN model

The internal temperature profile of APH plays a crucial role in determining the progression of fouling as it influences the chemical reactions and more importantly the location of ABS deposition zone within the APH. However, in absence of any sensors inside APH the operators remain blind to the fouling phenomena unfolding inside the matrix. Estimation of fouling propensity and identification of ABS deposition zone can assist the operator to make informed decisions about managing the fouling vis-a-vis the operating and maintenance costs it incurs.

Chen et al. (2020) have suggested a number that indicates the propensity of fouling within APH based on the temperatures and the gas composition (ammonia  $NH_3$  and sulfur oxide  $SO_3$ ). PINN developed above can be utilized not only for estimation of fouling propensity but also for identifying fouling deposition zone within APH. Localization of this fouling zone is critical because it moves with the internal temperature conditions and has a large influence on the overall health of APH. Typically, when this fouling zone is close to the gas exit, the deposits within it are removable by a cleaning equipment called soot blower. However, when this fouling zone moves away from gas exit due to a shift in temperatures, it increases the risk of APH clogging and ultimate forced outage of the plant. ABS deposition temperature depends on the concentration of  $NH_3$  and  $SO_3$  in the APH. It can be calculated using the empirical relation presented in eq. (26) (Huang, Sun, Chen, Li, Gu, Hu, & Cheng 2015).

$$T_{ABS} = 0.4059[\ln(\varphi_{NH_3}\varphi_{SO_3})]^2 + 11.45 \ln(\varphi_{NH_3}\varphi_{SO_3}) + 192.29 \quad (26)$$

Here,  $T_{ABS}$  represents initial condensation temperature of ABS in  $^{\circ}C$ ;  $\varphi_{NH_3}$  and  $\varphi_{SO_3}$  represents the concentration of  $NH_3$  and  $SO_3$  in ppm.

Fouling propensity indicator (R-Number) for ABS deposition tendency is given by eq. (27) (Chen et al. 2020). Here,  $\varphi_{NH_3,0}$  and  $\varphi_{SO_3,0}$  represents the reference concentrations of  $NH_3$  and  $SO_3$  in the flue gas at the inlet of the air preheater, respectively taken as 3 ppm and 5 ppm;  $T_{ABS}$  in K,  $T_{cold,bottom,avg}$  and  $T_{cold,top,avg}$  are the average temperature at the cold end of the APH in K, similarly  $T_{hot,bottom,min}$  and  $T_{hot,top,min}$  are the average temperature at the hot end of the APH in K.

$$R - number = \frac{\varphi_{NH_3}\varphi_{SO_3}}{\varphi_{NH_3,0}\varphi_{SO_3,0}} \frac{T_{ABS}-T_{cold,bottom,avg}}{T_{cold,top,avg}-T_{cold,bottom,avg}} \exp\left(\frac{T_{ABS}-T_{hot,bottom,min}}{T_{hot,top,min}-T_{hot,bottom,min}}\right) \quad (27)$$

Figure 4 represents the summary of steps required to perform online health monitoring of the APH. A prerequisite base PINN model can be trained offline for single set of boundary conditions and given design parameters (geometry, material properties) of APH. This model is then further used in online health monitoring by freezing the weights between input and first layer of the networks. In online conditions, boundary conditions change continuously and hence the internal temperature profile in APH change as well. To infer the internal temperature profile, transfer learning framework is used along with base PINN model to train the new PINN model corresponding to new boundary conditions. PINN model networks are used to predict the internal temperature profile in APH. Internal temperature profile is then used to estimate unremovable deposit region and fouling propensity. Insight of deposit region and fouling propensity can be used by operator to do suitable operation changes.

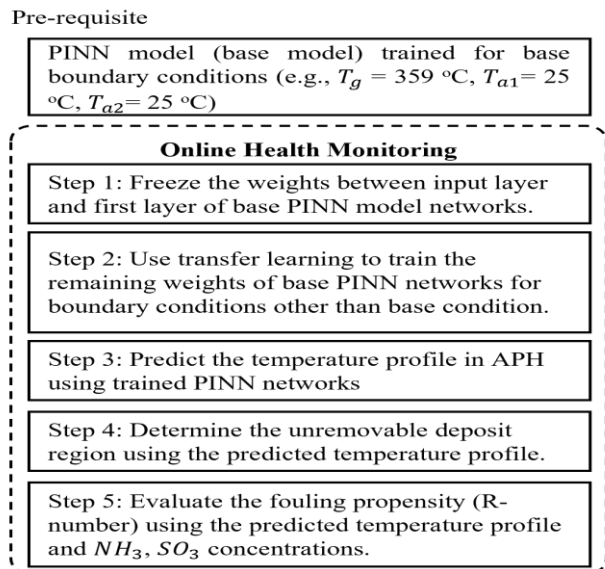


Figure 4 Flow chart for health monitoring using PINN

### 3. RESULTS AND DISCUSSION

#### 3.1. Base PINN and Numerical Solution comparison

Numerical solution of the governing equations for the APH is obtained using finite difference method described by Li (1983). The numerical solution was validated with experimental data earlier (Gupta et al. 2021). Design and material related parameter values of APH used for the simulation are mentioned in Appendix A.1. This numerical simulation is used as a benchmark for comparing predictions from PINN models. The base PINN model is trained for the same APH with inlet gas temperature as 359°C and inlet air temperature as 25°C. It is trained using the architecture mentioned in section 2.2. It uses 15000 collocation, 15000 boundary and 15000 sub-domain interface points for training. As shown in Figure 5 the base PINN is trained for 788 epochs to get an acceptable loss value. Training was stopped as per early stopping criteria (no improvement in total loss for last 100 epochs). Model weights were restored to best weights obtained corresponding to best loss value. Post training of the model, values of temperature for flue gas side, primary air side, secondary air side and the matrix are inferred. Comparison of temperature profiles obtained through numerical finite difference method and PINN model is presented in Figure 6. The top row shows the fluid temperature profiles; the middle row shows the metal matrix temperature profiles. For continuity, the three sub-domains gas, primary air and secondary air are connected at the interfaces in Figure 6. The region between  $\theta = 0-180^\circ$  represents gas domain,  $\theta=180^\circ-250^\circ$  represents primary air and  $\theta= 250^\circ-360^\circ$  represents secondary air. As seen in the figure, there is an excellent match between the two solutions. The base PINN solution has a mean absolute error of  $8.1e-3$  and a maximum absolute error of 0.03 when compared against the numerical solution for normalized value. It is equivalent to mean absolute error of  $2.7^\circ\text{C}$  and maximum absolute error of  $10^\circ\text{C}$  considering non-normalized solution. The domain decomposition technique also enabled capturing the thermal phenomena near the interfaces without any loss of accuracy. Although PINN requires a considerable time for training, its inference time is significantly lower than the numerical solution as shown in Table 1. The inference time of a trained PINN model will not deviate significantly even if the required granularity (mesh size) of the solution is altered. The same cannot be said about the numerical solution. Therefore, PINNs can be effectively used for soft sensing temperatures within APH in a near real-time scenario. The next challenge of making PINN work for varying boundary conditions is addressed in the next section.

Table 1 Training and Inference Time comparison for Numerical Method and PINN solution for Base Case

	Numerical Method	PINN
Training Time (sec)	N/A	4212
Inference Time (sec)	1076	1.8

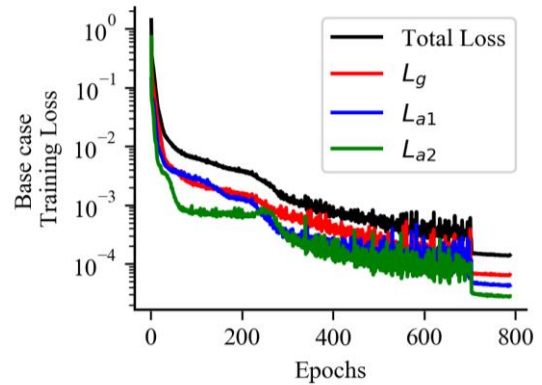


Figure 5 Training Loss for Base Case (Inlet Gas Temperature 359°C, Inlet Air Temperature 25°C)

#### 3.2. Training and inference for dynamic boundary condition

As discussed in section 2.3, the base PINN network with flue gas inlet temperature as 359°C and air inlet temperature as 25°C is used for training new PINNs for different boundary conditions via the transfer learning-based approach. The benefits of the approach are evaluated by testing it with a set of 9 different boundary conditions often encountered in industrial APH operation. The accuracy and the training - inference time for the transfer learning approach is compared with the corresponding numerical simulation as well as a PINN trained from scratch for the given boundary condition, as shown in Table 2. As seen, there is no loss of accuracy with the transfer learning approach when compared to PINN from scratch and the numerical simulation, validating its application. As the requirement is that of monitoring APH health in near real-time, the combined training and inference time of PINNs is compared against the inference time of a numerical solution (as it does not need any retraining). The premise here is that the PINN model will be trained online and used immediately for temperature predictions.

The training and inference time for a PINN trained from scratch typically exceeded the inference time required for a numerical simulation. However, a transfer-learned PINN adapted for a new boundary condition using the previously built base PINN brought down the training and inference time substantially compared to the numerical simulation. On an average the combined training and inference time for a transfer-learned PINN was 78% less than the corresponding inference time for the numerical simulation.

Industrial digital twins are increasingly using edge analytics for reducing the traffic and costs for cloud computations (Sánchez, Jörgensen, Törngren, Inam, Berezovskyi, Feng, Fersman, Ramli, & Tan 2021). Often the task of re-training of machine/deep learning models is allocated to cloud due to

intensive computational requirements and dependence on past historical data (which is stored on cloud). PINNs can help reduce the dependence on large quantities of data and a quick retraining framework such as this one can enable it to run on the edge instead of on cloud. This online retraining and near real-time predictions from the retrained model can provide an effective way of monitoring equipment health in industrial and manufacturing settings.

### 3.3. Health monitoring of APH using PINNs

Near real-time temperature predictions from PINN model can be effectively used for monitoring the risk posed by fouling. As an example, the internal temperatures predicted by PINN for the base case are used for calculating the fouling propensity and identifying the fouling zone as described in section 2.4. The fouling propensity is calculated assuming ammonia ( $\text{NH}_3$ ) and sulfur oxide ( $\text{SO}_3$ ) concentrations as 3 ppm and 10 ppm respectively. For this scenario,  $T_{ABS}$  calculated using eq. (26) is  $236.45^\circ\text{C}$  and R-number calculated using eq. (27) is 0.79. Figure 7 shows the maximum, minimum and average gas temperature profile in the axial direction against the depth of APH ( $z = 0$  indicates gas entry). The overall fouling zone for the given conditions is also indicated based on the calculated  $T_{ABS}$ . As seen in the figure a portion of this fouling zone falls beyond the reach of the cleaning soot blowing equipment and hence creating a

permanent deposit inside the APH. Under normal circumstances the operator is completely blind to this insight. However, with this estimation operator may take some corrective actions to decelerate the fouling.

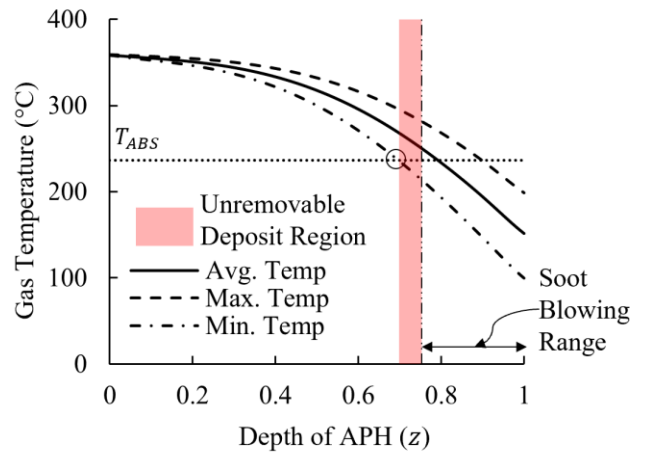


Figure 7 Gas Temperature distribution and Unremovable Deposit region in APH

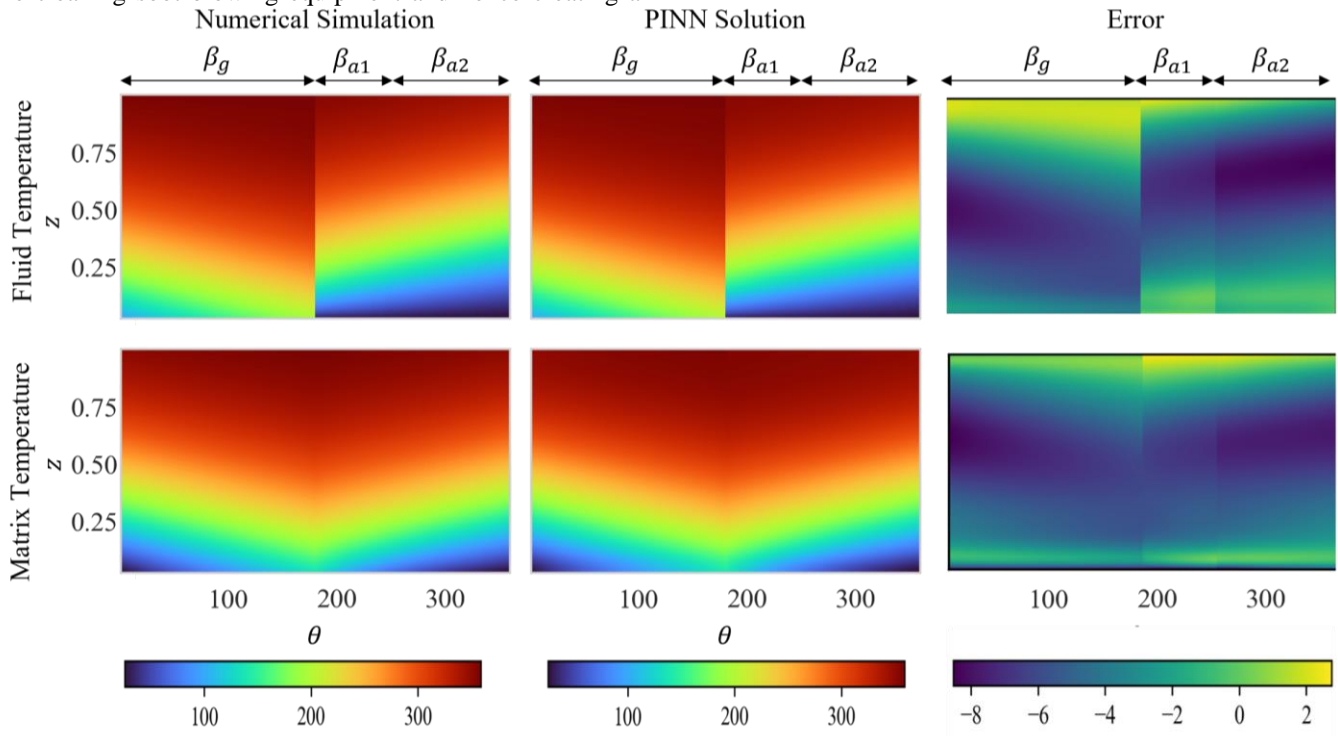


Figure 6 Comparison of PINN and Numerical Solution

Table 2 Comparison of inference time for Transfer Learning based Training of PINN and numerical simulation

Case	Inlet Gas Temperature BC	Inlet Air Temperature BC	Numerical Simulation	PINN trained with random initialization (without using the Base PINN)			Transfer Learning using the Base PINN		
			Inference time (sec)	Train time (sec)	Inference time (sec)	MAE (wrt to corresponding numerical simulation)	Train time (sec)	Inference time (sec)	MAE (wrt to corresponding numerical simulation)
1	329	19	1028	3716	3.6	0.012	211	3.5	0.0105
2	354	48	922	2782	3.7	0.005	255	3.8	0.0052
3	331	38	1122	3314	3.9	0.030	187	3.6	0.0098
4	330	31	915	3174	4.0	0.008	190	3.4	0.0105
5	390	36	1066	2895	3.5	0.007	194	3.5	0.0033
6	320	37	1076	2847	3.3	0.016	268	3.5	0.0112
7	399	23	1179	3370	3.7	0.011	194	3.6	0.0056
8	388	13	1188	2878	3.7	0.020	195	3.9	0.0021
9	363	43	1038	2726	3.7	0.016	181	3.7	0.0043

Figure 8 shows an example of effect of ammonia and ambient inlet air temperature on the fouling risk for APH. It is seen that high ammonia and low ambient temperature condition poses the greatest risk because of the formation of deep unremovable deposits within APH. The PINN model therefore can be used as an effective monitoring tool for APH predictive maintenance.

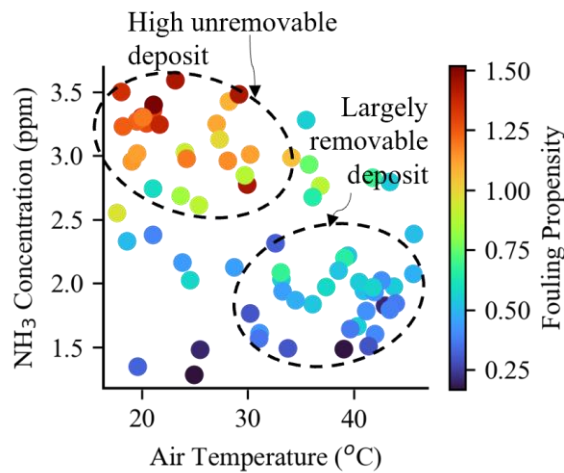


Figure 8 Fouling Propensity Monitoring

Although the PINN framework demonstrated here is certainly very useful, it can be improved and enhanced further to make it more effective. Firstly, the model can be modified to incorporate equations governing the chemical reactions and the deposition kinetics as well. Although the

model demonstrated in this work caters to dynamic inlet temperature conditions, it can be expanded to accommodate dynamic flow rates, material properties as well as APH geometries. This can pave the way for building a generic and adaptable PINN model for monitoring and predictive maintenance of APH. On the deep learning front, we plan to explore different methods for building an all-condition PINN model capable of handling dynamic changes without having to do extensive retraining.

#### 4. CONCLUSION

A Physics-informed Neural Network (PINN) is designed for capturing thermal phenomena in an air preheater (APH) used in thermal power plants. The APH is divided into three sub-domains and a separate deep neural network (DNN) is constructed for each of them. The base PINN model is trained by stitching the three DNNs together through a common loss function comprising of governing partial differential equations and continuity constraints at the sub-domain interfaces. Further, a transfer learning framework is used to enable quick training and inference from the PINN model for dynamically changing boundary conditions. The PINN model is shown to be faster than corresponding physics-based numerical solver, without appreciable loss of accuracy, making the model suitable for online and real-time applications. The predictions from the model are further used for estimating propensity of fouling in APH in near real-time, thereby assisting the operator in avoiding forced outages by taking informed decisions. The proposed PINN framework can be easily integrated into a digital twin of APH for a predictive maintenance application.

## ACKNOWLEDGEMENT

The current work was funded by Tata Consultancy Services Limited. The authors thank Mr. K. Ananth Krishnan, and Dr. Gautam Shroff for their encouragement and support. The authors would also like to thank Dr Shirish Karande, Dr Lovekesh Vig and Mr. Souridas A. for their inputs and suggestions.

## REFERENCES

- Baydin, A.G., Pearlmutter, B.A., Radul, A.A. & Siskind, J.M., (2018). Automatic Differentiation in Machine Learning: a Survey. *Journal of Machine Learning Research*, 1-43.
- Belbute-Peres, F.D.A., Chen, Y.F. & Sha, F., (2021). HyperPINN: Learning parameterized differential equations with physics-informed hypernetworks. *arXiv preprint arXiv:2111.01008*.
- Burke, J.M. & Johnson, K.L., (1982). Ammonium sulfate and bisulfate formation in air preheaters. *Final report Oct 80-Oct 81 (No. PB-82-237025)*. Radian Corp., Austin, TX (USA).
- Cai, S., Wang, Z., Wang, S., Perdikaris, P. & Karniadakis, G.E., (2021). Physics-Informed Neural Networks for Heat Transfer Problems. *Journal of Heat Transfer*, 143(6). doi:10.1115/1.4050542
- Cai, S., Mao, Z., Wang, Z., Yin, M. & Karniadakis, G.E., (2022). Physics-informed neural networks (PINNs) for fluid mechanics: a review. *Acta Mechanica Sinica*. doi:10.1007/s10409-021-01148-1
- Chakraborty, S. (2021). Transfer learning based multi-fidelity physics informed deep neural network. *Journal of Computational Physics*. doi:https://doi.org/10.1016/j.jcp.2020.109942
- Chen, X., Xu, S., Yang, Y., Wang, L.M. & Wang, D.D., (2020). Performance Analysis and Optimization of Flue Gas Waste Heat Recovery System of a 600MW Coal-Fired Power Plant. *ASME 2020 Power Conference*. doi:10.1115/POWER2020-16873
- Cuomo, S., Di Cola, V.S., Giampaolo, F., Rozza, G., Raissi, M. & Piccialli, F., (2022). Scientific Machine Learning through Physics-Informed Neural Networks: Where we are and What's next. *arXiv preprint arXiv:2201.05624*.
- Desai, S., Mattheakis, M., Joy, H., Protopapas, P. & Roberts, S., (2021). One-Shot Transfer Learning of Physics-Informed Neural Networks. *arXiv preprint arXiv:2110.11286*.
- Drobnic, B., Oman, J., & Tuma, M. (2006). A numerical model for the analyses of heat transfer and leakages in a rotary air preheater. *International Journal of Heat and Mass Transfer*, 5001-5009.
- Gupta, A., Jadhav, V., Patil, M., Deodhar, A. & Runkana, V., (2021). Forecasting of Fouling in Air Pre-Heaters Through Deep Learning. *ASME 2021 Power Conference*. doi:10.1115/POWER2021-64665
- Heidari-Kaydan, A., Hajidavalloo, E. & Mehrzad, S., (2021). Three-Dimensional Simulation of Leakages in Rotary Air Preheater of Steam Power Plant. *Heat Transfer Engineering*, 1-17. doi:10.1080/01457632.2021.1976563
- Heinlein, A., Klawonn, A., Lanser, M. & Weber, J., (2021). Combining machine learning and domain decomposition methods for the solution of partial differential equations—A review. *GAMM-Mitteilungen*. doi:10.1002/gamm.202100001
- Huang F-L, Sun Z-J, Chen R, Li P-C, Gu J-F, Hu Y-C, & Cheng G. (2015). The investigation of heat transfer model of regenerative air preheaters adapt to SCR denitrification. *Journal of Engineering Thermophysics*, 2683-2688.
- Jagtap, A.D., Kharazmi, E. & Karniadakis, G.E. (2020). Conservative physics-informed neural networks on discrete domains for conservation laws: Applications to forward and inverse problems. *Computer Methods in Applied Mechanics and Engineering*. doi:https://doi.org/10.1016/j.cma.2020.113028
- Jagtap, A.D. & Karniadakis, G.E., (2020). Extended physics-informed neural networks (xpinns): A generalized space-time domain decomposition based deep learning framework for nonlinear partial differential equations. *Communications in Computational Physics*, 28(5), 2002-2041.
- Lagaris, I.E., Likas, A. & Fotiadis, D.I., (1998). Artificial neural networks for solving ordinary and partial differential equations. *IEEE Transactions on Neural Networks*, 987-1000. doi:10.1109/72.712178
- Li, C.-H. (1983). A Numerical Finite Difference Method for Performance Evaluation of a Periodic-Flow Heat Exchanger. *J. Heat Transfer*, 611-617. doi:10.1115/1.3245629
- Menasha, J., Dunn-Rankin, D., Muzio, L. & Stallings, J., (2011). Ammonium bisulfate formation temperature in a bench-scale single-channel air preheater. *Fuel*, 2445-2453. doi:https://doi.org/10.1016/j.fuel.2011.03.006
- Moseley, B., Markham, A. & Nissen-Meyer, T., (2021). Finite Basis Physics-Informed Neural Networks (FBPINNs): a scalable domain decomposition approach for solving differential equations. *arXiv preprint arXiv:2107.07871*.
- Muzio, L., Bogseth, S., Himes, R., Chien, Y.C. & Dunn-Rankin, D., (2017). Ammonium bisulfate formation and reduced load SCR operation. *Fuel*, 206, 180-189. doi:https://doi.org/10.1016/j.fuel.2017.05.081
- Penwarden, M., Zhe, S., Narayan, A. & Kirby, R.M., (2021). Physics-Informed Neural Networks (PINNs) for Parameterized PDEs: A Metalearning Approach. *arXiv preprint arXiv:2110.13361*.
- Raissi, M., Perdikaris, P. & Karniadakis, G.E., (2019). Physics-informed neural networks: A deep learning framework for solving forward and inverse problems involving nonlinear partial differential equations.

*Journal of Computational Physics*, 686-707. doi:https://doi.org/10.1016/j.jcp.2018.10.045

Sánchez, J.M.G., Jörgensen, N., Törngren, M., Inam, R., Berezovskyi, A., Feng, L., Fersman, E., Ramli, M.R. & Tan, K., (2021). Edge computing for cyber-physical systems: A systematic mapping study emphasizing trustworthiness. *arXiv preprint arXiv:2112.00619*.

Shukla, K., Jagtap, A.D. & Karniadakis, G.E., (2021). Parallel physics-informed neural networks via domain decomposition. *Journal of Computational Physics*, 447. doi:https://doi.org/10.1016/j.jcp.2021.110683

Skiepko, T. (1988). The effect of matrix longitudinal heat conduction on the temperature fields in the rotary heat exchanger. *International Journal of Heat and Mass Transfer*, 31(11), 2227-2238. doi:10.1016/0017-9310(88)90155-X

Sundar, S., Rajagopal, M.C., Zhao, H., Kuntumalla, G., Meng, Y., Chang, H.C., Shao, C., Ferreira, P., Miljkovic, N., Sinha, S. & Salapaka, S. (2020). Fouling modeling and prediction approach for heat exchangers using deep learning. *International Journal of Heat and Mass Transfer*. doi:https://doi.org/10.1016/j.ijheatmasstransfer.2020.12.0112

Wang, H., Planas, R., Chandramowlishwaran, A. & Bostanabad, R., (2021). Train once and use forever: Solving boundary value problems in unseen domains with pre-trained deep learning models. *arXiv e-prints, arXiv--2104*.

Wang, L., Bu, Y., Li, D., Tang, C. & Che, D., (2019). Single and multi-objective optimizations of rotary regenerative air preheater for coal-fired power plant considering the ammonium bisulfate deposition. *International Journal of Thermal Sciences*, 136, 52-59. doi:https://doi.org/10.1016/j.ijthermalsci.2018.10.005

Zhou, C., Zhang, L., Deng, Y. & Ma, S.C., (2016). Research progress on ammonium bisulfate formation and control in the process of selective catalytic reduction. *Environmental Progress & Sustainable Energy*, 1664-1672. doi:https://doi.org/10.1002/ep.12409

## BIOGRAPHIES



**Vishal Jadhav** has completed his Master of Technology degree in Aerospace Engineering from Aerospace Department, IIT Madras, India in 2017. He is currently working as a Scientist at TCS Research with a focus on digital twin development for manufacturing and engineering domains.

He has more than 7 years of experience in applying machine and deep learning, computational fluid dynamics. He has filed several patents and has published research papers in reputed conference proceedings. His current research includes

combining physics and data based algorithms for industrial digital twins



**Anirudh Deodhar** is currently working as a scientist in TCS Research with a focus on manufacturing and engineering domains. He is a mechanical engineer and holds a master's degree from University of Cincinnati, USA. He has more than 10 years of experience in applying process modeling,

computational fluid dynamics, machine/deep learning for industrial digital twins. He is a member of American Society of Mechanical Engineers (ASME). He has published in several international journals and conferences and has filed more than 15 patents. His current research includes fusing physics and deep learning for industrial cyber physical systems.



**Ashit Gupta** has completed his Master of Technology degree in Aerodynamics from Aerospace Department, IIT Bombay, Mumbai, India in 2017. He has been working as a researcher at Tata Research Development & Design Centre for the past 4.5 years. His expertise lies in machine

learning & deep learning and has contributed towards research for process and manufacturing industries. He has filed several patents and has published research papers in reputed journals and conference proceedings (IEEE, ASME etc.). He has provided solutions like long-term forecasts of health conditions for APH, optimization of operation of boilers in thermal power plants, performance prediction in rotary kiln etc. His interest lies in physics informed deep learning for industrial equipment.



**Dr Venkataramana Runkana** is currently the Chief Scientist and Head of the Research & Innovation Programme for Manufacturing & Engineering in TCS. He is a chemical engineer by education and holds a Ph.D. from Columbia University, New York. He has more than 30 years of

experience in process modeling, simulation and optimization, advanced data analytics and digital twins, process development, scale-up and design, nanomaterials, and drug delivery systems. He received the TCS Distinguished Scientist Award in 2014 and was an AICTE-INAE Distinguished Visiting Professor at IIT Kanpur during 2013-2018.

**APPENDIX**

A.1 APH Design and Operational data for base case PINN

Parameter	Values
<b>Matrix</b>	
Inner radius (m)	1.63
Outer radius (m)	8.21
Height of matrix (m)	2.05
<b>Sector Angles</b>	
$\beta_g$	180°
$\beta_{a1}$	70°
$\beta_{a2}$	110°
<b>Material Properties</b>	
Thermal conductivity (W/mK)	52.92
Heat capacity (J/kgK)	456
<b>Gas</b>	
Inlet temperature (°C)	359
Flow rate (kg/s)	770
<b>Primary Air</b>	
Inlet temperature (°C)	25
Flow rate (kg/s)	452.53
<b>Secondary Air</b>	
Inlet temperature (°C)	25
Flow rate (kg/s)	268.13